RSC Advances

PAPER

View Article Online
View Journal | View Issue

Cite this: *RSC Adv.*, 2017, **7**, 39204

Highly promoted removal of Hg(II) with magnetic $CoFe_2O_4$@SiO_2 core–shell nanoparticles modified by thiol groups

He Zhu, Yi Shen, Qin Wang, Kuan Chen, Xi Wang, Ganwei Zhang, Jingjing Yang, Yongfu Guo* and Renbi Bai*

A simple and environmentally friendly material, $CoFe_2O_4$@SiO_2–SH, was prepared successfully with $CoFe_2O_4$ nanoparticles coated by SiO_2 which was further functionalized with thiol groups (–SH). $CoFe_2O_4$@SiO_2–SH nanoparticles were structurally and thermally characterized. The results show that the additive of 3-mercaptopropyltriethoxysilane was successfully grafted onto $CoFe_2O_4$@SiO_2. The affecting factors, including pH, adsorbent dosage, and the initial concentration of Hg Hg(II) and coexisting ions were fully investigated and well elucidated. The fitting of adsorption kinetics and isotherm model indicated a good match with pseudo-second-order kinetics and Freundlich models. The Langmuir adsorption capability realized 641.0 mg g^{-1}. The data of thermodynamics illustrated that the removal for Hg(II) was exothermic and spontaneous. Last, an application evaluation of the material was also carried out. The adsorbent can achieve a quick and effective separation *via* a magnetic field after adsorption. Hence, the $CoFe_2O_4$@SiO_2–SH material will be a favorable and promising adsorbent to remove Hg(II) from water.

Received 2nd June 2017
Accepted 5th August 2017

DOI: 10.1039/c7ra06163c

rsc.li/rsc-advances

1. Introduction

With the economic globalization and the large-scale development of industrialization, water pollution of heavy metals caused by a large amount of sewage from chemical plants and mining fields, has attracted a lot of research attention. Mercury, one of the most toxic pollutants exhibiting properties of persistence, bioaccumulation and migration,[1] can enter the human body through the food chain, causing irreversible serious damage to human body function and the nervous system.[2]

In many countries, mercury pollution incidents occur frequently.[3] In the 1980s in China, several serious mercury pollution incidents, occurring along the Songhua River, in the lower reaches of Tianjin Jiyun River and Jinzhou Bay in Liaoning Province, *etc.* greatly attracted people's attention. So, it is imperative to solve the problem of mercury pollution in water.

To solve this issue, there are many methods developed for the recovery of mercury, such as precipitation, ion exchange, physical separation and microbiological method and so on.[4–7] Nevertheless, these technologies always have shortcomings like poor removal capacity, low metal removal efficiency and the risk of secondary pollution.[8] Hence, it is necessary to explore economic and effective technologies to treat the pollution. Adsorption has been recognized as an economic and highly effective method used in water treatment due to its cost-effective and efficient.[9] However, most of adsorbent materials have some issues like poor regeneration, easy to produce secondary pollution and poor selectivity. Especially after the completion of the adsorption, the material is difficult to be separated from water, which is the most difficult problem to apply on the real projects.

MFe_2O_4 (M represents metal elemental), a kind of magnetic substance with a cubic spinel structure, has well received by the people's favorites and been widely used in many fields.[10] Among them, $CoFe_2O_4$ gets more attention due to its advantages, such as large saturation magnetization and good thermal stability. Fe_3O_4 was also one of magnetic materials and got more modification and researches in recent years.[11–13]

Compared with the production process of Fe_3O_4, the synthesis method of $CoFe_2O_4$ is simpler and the process of reaction can underway without the need of nitrogen environment. According to the study of Zhang,[14] the number of hydroxyl group (M–OH) on the surface of $CoFe_2O_4$ (38.1%) was higher than that of Fe_3O_4 (25.4%). The amount of M–OH has a significant effect on the performance of the adsorbents, and the more M–OH, the more easily material can be modified.

In addition to the above advantages, $CoFe_2O_4$ also has some shortcomings that cannot be overcome by itself, such as easy agglomeration, corrosion in acidic environments and so on, which is not conducive to the material adsorption and adsorption selectivity. In general, the methods of adding surfactant or

Center for Separation and Purification Materials &Technologies, Suzhou University of Science and Technology, Suzhou 215009, P. R. China. E-mail: yongfuguo@163.com; Tel: +86-512-68092987

forming silica layer outside $CoFe_2O_4$ through hydrolyzing tetraethyl silicate (TEOs) can greatly improve corrosion resistance and dispersion of $CoFe_2O_4$ in water.[15,16]

According to the Lewis acid–base interactions,[17] thiol group and mercury should have a high affinity to each other, for thiol group is characteristic of soft base and mercury is a soft acid. Thiol group is also an excellent ligand. $CoFe_2O_4$ can be modified with thiol group to improve the adsorption properties of materials. 3-Mercaptopropyltrimethoxysilane (MPTMS) is a silane coupling agent containing mercapto functional groups. After the inorganic layer SiO_2 was coated on the surface of $CoFe_2O_4$ and MPTMS was added, the mercapto group was successfully grafted.

During the process of modification, the contents of thiol in adsorbents are related to amount of catalysts used in the reaction, the choice of solvents, reaction temperature and reaction time.[18]

Currently, most of magnetic adsorption materials were modified with Fe_3O_4. However, the research with $CoFe_2O_4$ modified materials to remove heavy metal was little. One aim of this paper is to explore the adsorption performance of the prepared adsorbent modified with other magnetic base material, *i.e.*, $CoFe_2O_4$; another aim is to prepare $CoFe_2O_4$ base adsorbent with core–shell construction and investigate its adsorption performance for Hg(II) ions when the prepared adsorbent was modified by thiol group.

So, in this paper, in order to overcome the defect of easy agglomeration and corrosion of $CoFe_2O_4$, improve its dispersion in water and simultaneously develop a novel adsorbent with high adsorption capability, a thiol-functionalized and silica-coated magnetic nanoparticle ($CoFe_2O_4$@SiO_2–SH) was synthesized by a simple method and employed to remove Hg(II) ions from water. The characteristics and properties of materials before and after modification were discussed by various means of characterization. To deeply comprehend the adsorption process of materials, the adsorption kinetics, isotherm and thermodynamics were employed. The effects of foreign ions on the adsorption process and the adsorption mechanism were discussed.

2. Materials and experimental methods

2.1 Experimental materials

Cobaltous nitrate hexahydrate ($Co(NO_3)_2 \cdot 6H_2O$), iron(III) acetylacetonate ($Fe(acac)_3$), ethylene glycol (EG), sodium acetate anhydrous (CH_3COONa), polyethylene glycol, cetyltrimethylammonium bromide (CTAB, 99 wt%), methanol (CH_3OH), glycerol ($C_3H_8O_3$) and ammonia water ($NH_3 \cdot H_2O$, 25–28 wt%) were provided by Sinopharm Chemical Reagent Co., Ltd. (China). (3-Mercaptopropyl)trimethoxysilane (MPTMS, 98 wt%) and TEOs were obtained from Macklin Reagent (China). All chemical materials and solvents were analytical grade.

2.2 Preparation of $CoFe_2O_4$@SiO_2–SH

2.2.1 Preparation of $CoFe_2O_4$. $CoFe_2O_4$ magnetic nanoparticles (MNPs) were obtained *via* using a hydrothermal technology. Briefly, $Co(NO_3)_2 \cdot 6H_2O$ (2.1825 g) and $Fe(acac)_3$ (5.2977 g) were dissolved in EG (90 mL), vigorous stirring for 30 min. Then, CH_3COONa (6.51 g) and polyethylene glycol (2.00 g) were added slowly under vigorous magnetic stirring until a uniform state was formed. The homogeneous solution was transferred into an autoclave (150 mL) and reacted in the oven at 453 K for 14 h. The resulting black mixture was washed with ultrapure water for several times after cooling, and finally dried at 333 K for 8 h and bagged for later use.

2.2.2 Preparation of $CoFe_2O_4$@SiO_2 MNPs. CTAB (0.1366 g) was dispersed in pure water (150 mL) as a surfactant by sonication for 20 min, and then $CoFe_2O_4$ (0.30 g) was dispersed in the above solution by vigorous mechanical stirring to form a uniform state. TEOs (1 mL) and $NH_3 \cdot H_2O$ (1.3 mL) were added as the catalysts at the temperature of 353 K and the reaction was continued for 3 h under mechanical stirring. The synthesized $CoFe_2O_4$@SiO_2 MNPs were separated magnetically, washed with ultrapure water for three times and dried at 333 K for 8 h. The obtained powder was calcined in a muffle furnace at 673 K for 4 h, and subsequently treated with HCl (1 M) for 12 h and continued to dry for later use.

2.2.3 Preparation of $CoFe_2O_4$@SiO_2–SH MNPs. In a typical preparation (Fig. 1), the obtained $CoFe_2O_4$@SiO_2 MNPs (0.2 g), CH_3OH (25 mL) and $C_3H_8O_3$ (150 mL) were added in a three-necked flask and stirred 30 min under a nitrogen atmosphere. Subsequently, the temperature was raised to 343 K and $NH_3 \cdot H_2O$ (2 mL) was added. The ligand MPTMS (0.3 mL) dissolved in CH_3OH (25 mL) was added dropwise under stirring. The mixture was allowed to react for 1 h under a nitrogen atmosphere at 343 K. After that, the reaction was continued for 5 h without nitrogen. The synthesized $CoFe_2O_4$@SiO_2–SH MNPs were separated magnetically and washed with ethanol and ultrapure water for three times, separately. The obtained powders were dried in vacuum at 333 K for 8 h.

2.3 Sample characterizations

The obtained samples were characterized *via* Scanning Electron Microscope (SEM), Transmission Electron Microscopy (TEM), X-ray Diffraction analysis (XRD), Fourier Transform Infrared (FT-IR), Vibrating Sample Magnetometer (VSM), N_2 adsorption–desorption isotherms, X-ray Photoelectron Spectroscopy (XPS) and Inductively Coupled Plasma Optical Emission Spectroscopy (ICP-OES). SEM (FEI Quanta FEG250, USA) and TEM (JEM-2100F, Japan) were used to observe the morphology. XRD (D/MAX-2550-18KW, Japan) was used to analyze the phase and crystallinity of the adsorbents.

The functional groups in materials were analyzed by FT-IR (Thermo, Nicolet-6700, USA). The magnetic property of the nanocomposites was confirmed by VSM (Quantum design, MPMS3, USA). The specific surface values and the pore distributions were got on the basis of nitrogen adsorption (Quanta, Autosorb-IQZ-MP-XR-VP, USA) at 77 K through using Brunauer–Emmett–Teller (BET) equation. Chemical elements compositions were measured by XPS (Thermo Scientific, Escalab 250Xi, USA). Quantitative determination of the contents for Hg(II) ions were performed by ICP-OES.

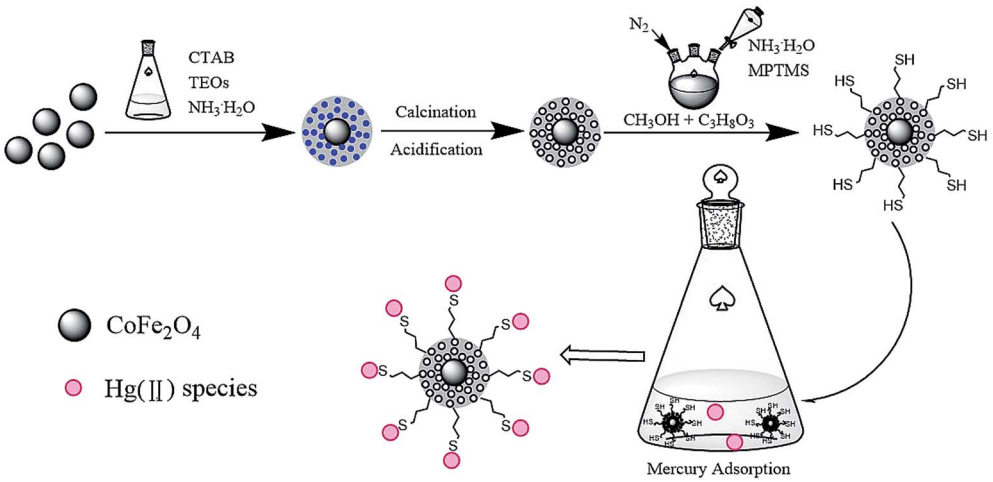

Fig. 1 Synthesized schematic of materials.

2.4 Adsorption experiments

To prevent the hydrolysis of mercury ions, the protective solution was configured as following: concentrated HNO_3 (10 mL) and HCl (0.1 mL) were added into ultrapure water (1000 mL). A reserve solution of Hg(II) (1 g L^{-1}) was made through dissolving $HgCl_2$ (0.6767 g) in a 500 mL protective solution. The protective solution was diluted with according to the desired concentration before each experiment.

The adsorption capacities of $CoFe_2O_4$@SiO_2–SH MNPs were evaluated at various conditions of pH, adsorbent dosages, contact time (t), initial concentration of Hg(II) and co-existing ions. Effect of pH values of 2–10 was assessed through adding 0.1 mol L^{-1} HCl and 0.1 mol L^{-1} NaOH solutions. Adsorption studies were carried out in 250 mL stoppered flaskets with Hg(II) solution (100 mL, 40 mg L^{-1}) and 0.005 g of adsorbents. The stoppered flaskets with the mixture were put in a shaker at 298 K for 12 h. The contents of Hg(II) were filtered *via* a 0.45 μm filter membrane and analyzed by ICP-OES. All of the tests were made in triplicate and the mean value was chosen for further analysis.

The dosage effects of adsorbents (defined as ratios of solid to liquid) were investigated at the intervals of 0.03, 0.05, 0.08, 0.1 and 0.15 g L^{-1} with 40 mg L^{-1} of Hg(II) at pH = 8 and 298 K. The contact time was examined at 1, 3, 5, 10, 30, 60, 180, 240, 300, 360, 420, 480, 540, 600, 660 and 720 min with 40 mg L^{-1} of Hg(II) and 0.005 g adsorbents at pH of 8 and 298 K.

The isotherms were studied at 298, 308 and 318 K at pH = 8 and t = 12 h. The initial concentration was charged between 20 and 200 mg L^{-1}. In the research of co-existing ions, five kinds of salts with a concentration of 10 mM and 100 mM were separately added into the Hg(II) solutions, respectively. The adsorption capacities can be determined as following:

$$q_e = \frac{(C_0 - C_e)}{W} \times V \quad (1)$$

here, q_e is the equilibrium capacity of Hg(II) (mg g^{-1}). C_0 and C_e are the initial and equilibrium concentration of Hg(II) (mg L^{-1}), separately. V and W are the solution volume (L) and adsorbent dosages (mg), separately.

3. Results and discussion

3.1 Characterization

SEM images of $CoFe_2O_4$, $CoFe_2O_4$@SiO_2 and $CoFe_2O_4$@SiO_2–SH MNPs are compared and shown in Fig. 2. The diameters of these adsorbents were about 50–90, 70–120, and 80–130 nm, respectively. As displayed in Fig. 2(a), the size of $CoFe_2O_4$ nanoparticles was small, but not uniform. Its surface was not smooth and crowded together. The observed aggregation may be due to the small size and the priority requirement for reducing the interfacial energy of nanoparticles.[19]

As displayed in Fig. 2(b), the size of $CoFe_2O_4$@SiO_2 became larger and the surface got smooth, indicating that $CoFe_2O_4$ successfully covered the silicon shell. Fig. 2(c) shows that the dispersity of the material had been greatly improved after modified by MPTMS. Based on the data in Fig. 2(d), the black magnetic core was wrapped around the translucent polymer coating, which was the silicon shell.

Fig. 3(a) shows the XRD patterns of $CoFe_2O_4$, $CoFe_2O_4$@SiO_2 and $CoFe_2O_4$@SiO_2–SH. It can observe that XRD pattern of $CoFe_2O_4$ had the diffraction peaks that appeared at $2\theta = 30.1°$, 35.5°, 43.3°, 53.8°, 56.8° and 62.5°, corresponding to the JCPDS file of $CoFe_2O_4$ (no. 22-1086).[20] All of the diffraction peaks of $CoFe_2O_4$@SiO_2 and $CoFe_2O_4$@SiO_2–SH were similar to those of $CoFe_2O_4$, and no peaks of any other phases were observed, indicating that the structure and the crystal formation of $CoFe_2O_4$@SiO_2 and $CoFe_2O_4$@SiO_2–SH MNPs remained unchanged after silicon-covering and thiol-functionalized process.[21]

The average sizes of $CoFe_2O_4$, $CoFe_2O_4$@SiO_2 and $CoFe_2O_4$@SiO_2–SH were calculated using the Debye–Scherrer formula to be 18.1, 20.0 and 21.6 nm, respectively.

The functional groups and chemical bonds in the materials were analyzed by means of FT-IR. Fig. 3(b) indicates FT-IR spectra of $CoFe_2O_4$, $CoFe_2O_4$@SiO_2 and $CoFe_2O_4$@SiO_2–SH ($CoFe_2O_4$@SiO_2–SH-1 was the fresh original sample and $CoFe_2O_4$@SiO_2–SH-2 was prepared one month ago). Broad FT-IR peaks around at 3439 and 1636 cm^{-1} observed should be

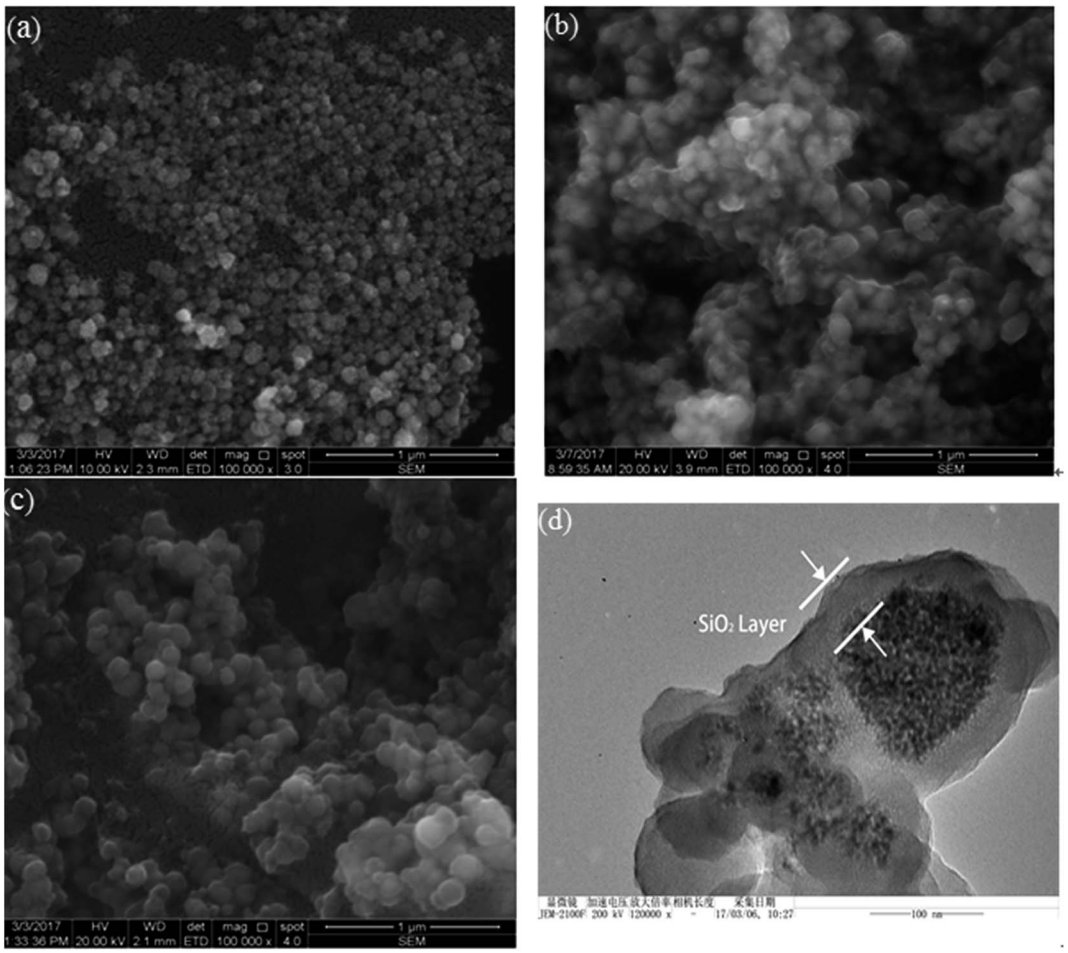

Fig. 2 SEM pictures of (a) $CoFe_2O_4$, (b) $CoFe_2O_4$@SiO_2, (c) $CoFe_2O_4$@SiO_2–SH and TEM image of (d) $CoFe_2O_4$@SiO_2–SH.

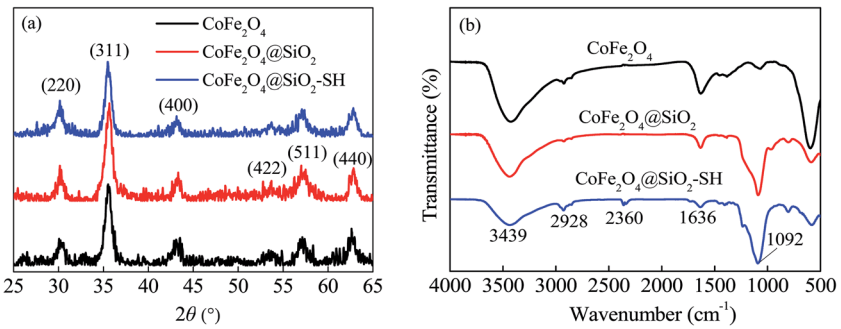

Fig. 3 XRD pictures (a) and FT-IR spectra (b) of $CoFe_2O_4$, $CoFe_2O_4$@SiO_2 and $CoFe_2O_4$@SiO_2–SH.

attributed to stretching vibration of –OH in surface adsorbed water.[22]

A broad adsorption band at 1092 cm^{-1} can be attributed to Si–O–Si.[23] As reported, typical adsorption bands of thiol group should be at about 2550 cm^{-1}. However, the two very weak peaks of –SH can be found at round 2360 cm^{-1}. It may be owing to the aggregation of –SH group and the effect of –H bonds. The phenomenon has also been reported by other scholars.[24,25] A bend at 2928 cm^{-1} was the C–H stretching of methylene from alkyl chain,[26] which can indirectly indicate that MPTMS had been successfully grafted onto $CoFe_2O_4$@SiO_2.

Moreover, the material of $CoFe_2O_4$@SiO_2–SH-2 had a similar FT-IR picture compared to the $CoFe_2O_4$@SiO_2–SH-1, shown in Fig. 3(b), which indicated that the prepared nanocomposite of $CoFe_2O_4$@SiO_2–SH had a good stability.

Fig. 4 shows the magnetic hysteresis loops of the three synthesized nanoparticles. The results show that saturation magnetization values for the three synthesized nanoparticles

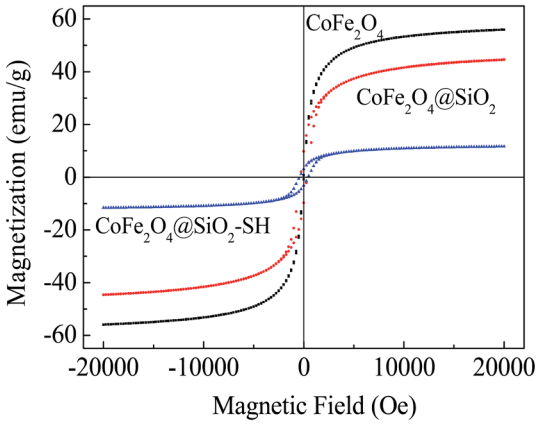

Fig. 4 VSM analysis of three synthesized materials.

were 56.03, 44.68 and 11.61 emu g^{-1} at 20 kOe, respectively. It can be clearly seen that the saturation magnetization values were decreased after modified by MPTMS, which indirectly proved that the surface of $CoFe_2O_4$@SiO_2 formed a non-magnetic thiol functional layer. After modified with MPTMS, the magnetic properties of the materials reduced obviously, but still can be easily separated from water *via* a magnetic field. It is conducive to the solid–liquid separation, making the whole adsorption process more environmentally friendly.

Based on the data in Fig. 5, the BET values, pore volumes and pore diameters of the three synthesized materials can be determined and exhibited in Table 1. From Table 1, the pore diameters and total pore volumes of $CoFe_2O_4$@SiO_2 changed little under the addition of surfactant CTAB and introduction of silicone shell TEOs. However, the BET value of $CoFe_2O_4$@SiO_2 is four times more than that of $CoFe_2O_4$, which may be the structure change of porous fluffy state of $CoFe_2O_4$@SiO_2 and the removal of CTAB after calcination at high temperature.

After the introduction of mercapto groups by MPTMS, the BET value returned to the original value, which may be due to the existence of large amount of organic mercapto groups grafted into $CoFe_2O_4$@SiO_2 mesopores.[27] On one hand, it shows the successful grafting of –SH; on the other hand, it indicates that the BET value was not the main factor affecting the adsorption performance of $CoFe_2O_4$@SiO_2–SH.

Table 1 Structure and chemical data of prepared mesoporous materials

Samples	BET values (m^2 g^{-1})	Total pore volumes (cm^3 g^{-1})	Pore diameters (nm)
$CoFe_2O_4$	48.49	0.424	3.413
$CoFe_2O_4$@SiO_2	225.36	0.552	3.062
$CoFe_2O_4$@SiO_2–SH	48.90	0.348	3.409

The wide-scan XPS spectra of the three synthesized materials are shown in Fig. 6. The elements of Fe, Co, O and C on the surface of $CoFe_2O_4$ were detected. For $CoFe_2O_4$@SiO_2, the peaks of Fe and Co elements almost disappeared, and the peaks of Si and S appeared, indicating that the silicon shell has completely wrapped the magnetic core $CoFe_2O_4$.

After modification with MPTMS, the peaks of Si became weak and a new peak of S appeared. Through high resolution scans of $CoFe_2O_4$@SiO_2–SH shown in Fig. 6(b)–(f), it can be known that the peaks of Fe 2p, Co 2p, C 1s, Si 2p and O 1s were at 724.59 eV, 781.86 eV, 284.33 eV, 101.73 eV and 531.92 eV, respectively, which directly indicated that the –SH was introduced onto the material successfully by MPTMS modification. The results agreed well with the FT-IR analysis of the sorbents.

3.2 Adsorption experiments

3.2.1 Effect of MPTMS. The addition of MPTMS had an obvious effect on the morphological and adsorption properties of $CoFe_2O_4$@SiO_2–SH. The relationship between the addition of MPTMS and the effects of adsorbents on mercury adsorption is shown in Fig. 7.

The adsorption capacity of $CoFe_2O_4$@SiO_2–SH increased with the increasing amount of the MPTMS under the condition of low addition of MPTMS. The optimum amount of MPTMS was found to be 0.3 mL. If the amount of MPTMS was less than 0.3 mL, the surface of the material would not be completely grafted by –SH group, therefore, the adsorption capacity cannot be maximized. When the addition amount of MPTMS was 0.3 mL, the q_e of adsorbents reached 374.4 mg g^{-1}.

Continued to increase the amount of MPTMS, the adsorption capacity of the adsorbents had not been further improved, but slightly decreased. So, the optimal amount of MPTMS

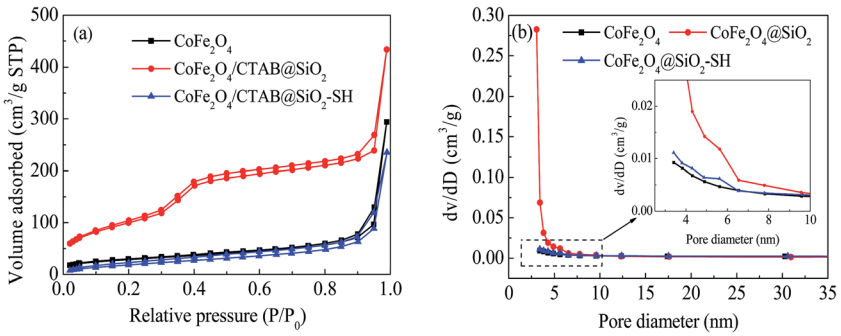

Fig. 5 N_2 adsorption desorption isotherms (a) and size distribution (b) of $CoFe_2O_4$, $CoFe_2O_4$@SiO_2 and $CoFe_2O_4$@SiO_2–SH.

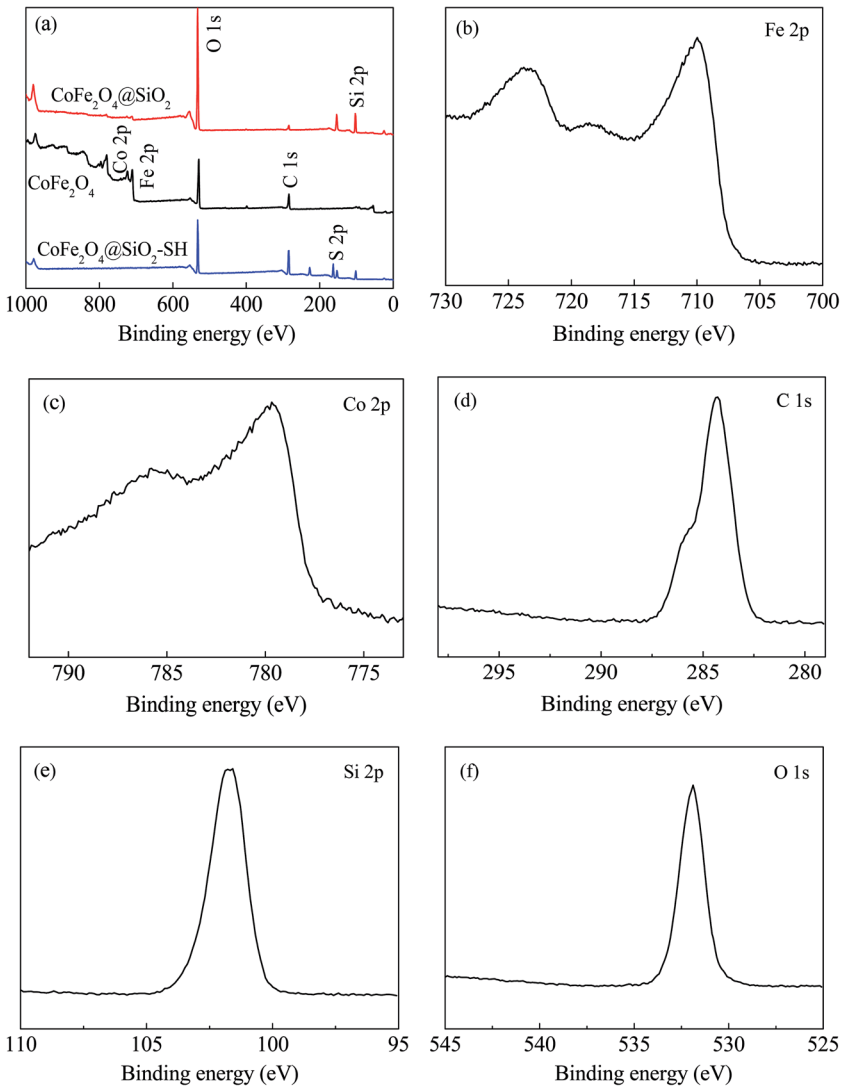

Fig. 6 XPS scan of (a) survey scan of $CoFe_2O_4$, $CoFe_2O_4$@SiO_2 and $CoFe_2O_4$@SiO_2–SH; high resolution scan of $CoFe_2O_4$@SiO_2–SH of (b) Fe 2p, (c) Co 2p, (d) C 1s, (e) Si 2p and (f) O 1s.

should be 0.3 mL. The reason may be owing to no excess active sites grafting with MPTMS on the surface of $CoFe_2O_4$@SiO_2. It also may be owing to the aggregation of magnetic core because of the uncontrolled self-condensation of trimethoxysilane groups, as Sun *et al.* reported.[28]

3.2.2 Effect of pH. For the value of pH can directly influence the interaction between H^+/OH^- and other substances, the existential morphology of mercury ions and the number of active sites on the surface of adsorbents, it is greatly important to explore the effects of solution pH on the adsorption capacity of $CoFe_2O_4$@SiO_2–SH. The pH value of solution was adjusted from 2 to 10 with C_0 of 40 mg L^{-1} at 298 K.

Based on the data from Fig. 8, q_e of $CoFe_2O_4$@SiO_2–SH for Hg(II) reached a maximum of 374.4 mg g^{-1} at pH of 8. Furthermore, the $CoFe_2O_4$@SiO_2–SH exhibited better adsorption performance at pH of 2–10. The adsorption capacity had also a high value of 271.2 mg g^{-1} even at pH = 2.

3.2.3 Effect of dosage. The optimum amount of adsorbents was selected by adding various amounts of adsorbents under the same adsorption conditions to test its adsorption effect. Different mass amounts of $CoFe_2O_4$@SiO_2–SH (3, 5, 8, 10 and 15 mg) were employed with 100 mL of Hg(II) (C_0 = 40 mg L^{-1}) in a water bath at pH = 8 and T = 298 K for 12 h.

As shown in Fig. 9, along with the increasing addition of $CoFe_2O_4$@SiO_2–SH, the adsorption capacity for Hg(II) decreased quickly and the adsorption efficiency increased remarkably. Fig. 9 shows that $CoFe_2O_4$@SiO_2–SH had great high adsorption capacities for Hg(II) even with pretty low dosage, for instance, 0.05 g L^{-1}.

3.3 Adsorption kinetics

The adsorption kinetic data of heavy metal ions were analyzed by testing pseudo-first-order (eqn (2)),[29] pseudo-second-order (eqn (3))[30] and the intra-particle diffusion models (eqn (4)).[31]

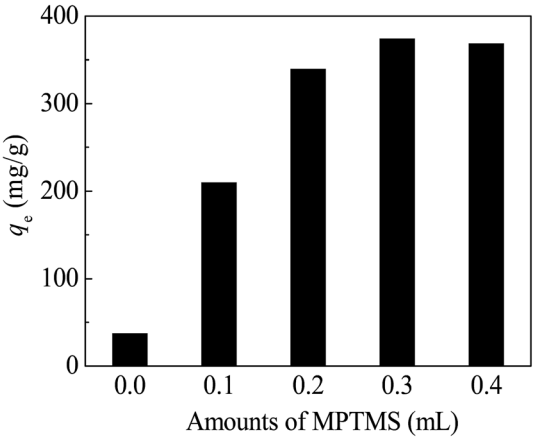

Fig. 7 Effect of MPTMS amount in $CoFe_2O_4$@SiO_2–SH. Conditions: pH = 8, dosage of 0.05 g L^{-1}, C_0 = 40 mg L^{-1}, t = 12 h and T = 298 K.

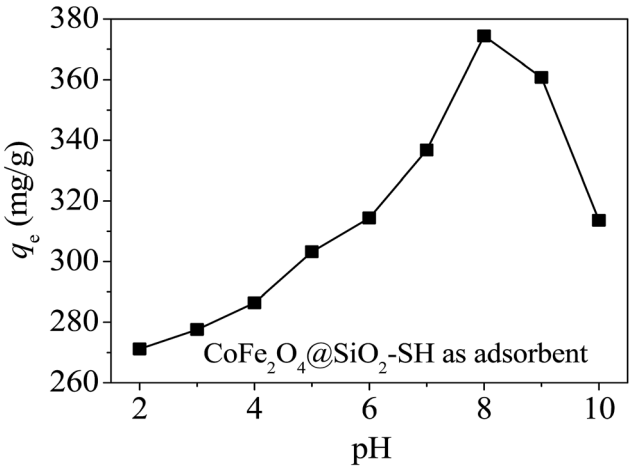

Fig. 8 Effects of pH on the removal of Hg(II) with $CoFe_2O_4$@SiO_2–SH as adsorbent. Conditions: dosage of 0.05 g L^{-1}, C_0 = 40 mg L^{-1}, t = 12 h and T = 298 K.

$$\ln(q_e - q_t) = \ln q_e - k_1 t \quad (2)$$

$$\frac{t}{q_t} = \frac{1}{q_e^2 k_2} + \frac{t}{q_e} \quad (3)$$

$$q_t = k_{di} t^{0.5} + C_i \quad (4)$$

Thereinto, k_1 (min^{-1}), k_2 (g mg^{-1} min) and k_{di} (mg g^{-1} $min^{0.5}$) are rate constants, respectively. q_t (mg g^{-1}) is instantaneous adsorption capacity at time of t, and C_i (mg g^{-1}) represents the thickness of boundary layer.

The diffusion and chemisorption are normally regarded as the rate limiting step by pseudo-first-order and pseudo-second-order models, separately. The Weber and Morris diffusion is used to analyze the suitability and effectiveness of the adsorption process. Fig. 10(a) shows that when $t \leq 60$ min, the adsorption rate was very fast, which may be due to the surface of the material had a rich activity of adsorption sites at the beginning of the reaction. With the passage of time, more and more Hg(II) was adsorbed onto the materials, and meanwhile, the concentration gradient between the surface of the material and the interior of solution decreased, resulting in a decreasing adsorption rate, and ultimately tending to a balance.

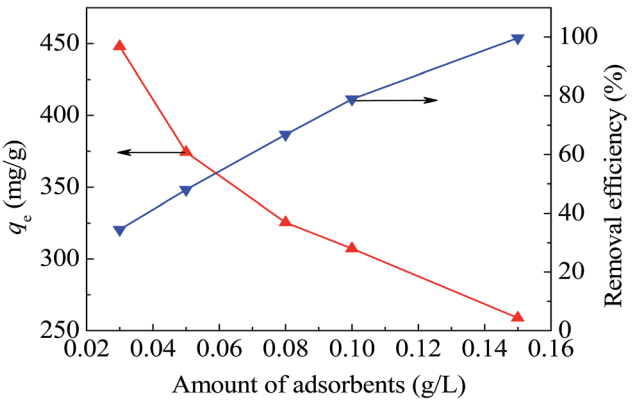

Fig. 9 Effects of dosage with $CoFe_2O_4$@SiO_2–SH as adsorbent. Conditions: pH = 8, C_0 = 40 mg L^{-1}, t = 12 h and T = 298 K.

The goodness of fitting was estimated from the measurement coefficient R^2. The calculated results were listed in Table 2. The data from pseudo-first-order model in Fig. 10(b) did not show good agreement (R^2 = 0.941) with the experimental data, and the difference between the theoretical $q_{e,cal}$ (332.8 mg g^{-1}) and the experimental $q_{e,exp}$ (374.4 mg g^{-1}) was a little large. The data from pseudo-second-order model in Fig. 10(c) fitted well (R^2 = 0.989), and the theoretical $q_{e,cal}$ (392.2 mg g^{-1}) was close to the actual $q_{e,exp}$. Therefore, the experimental results can be well represented by pseudo-second-order model and indicated that the removal of Hg(II) with $CoFe_2O_4$@SiO_2–SH involved chemical reaction.

In Fig. 10(d), the initial linear portion represented instantaneous adsorption on the surface of the material, indicating that the mass transfer in the early stage was achieved by large pore diffusion. The second stage was the gradual adsorption, indicating that mass transfer at this stage was achieved *via* microporous diffusion. The second stage was the main diffusion rate limitation. The third line was tending to equilibrium stage. Straight lines did not go through the origin, indicating that intra-particle diffusion was not the only rate limitation.

3.4 Adsorption isotherms

To further investigate the capacity of Hg(II) onto $CoFe_2O_4$@SiO_2–SH, Langmuir (eqn (5))[32] and Freundlich models (eqn (7))[33] were employed. The Langmuir model supposes the adsorption as monolayer and occurring on a homogeneous surface shown as eqn (5), whereas Freundlich model is built on the theory of multilayer adsorption shown as eqn (6).

$$\frac{C_e}{q_e} = \frac{C_e}{Q_m} + \frac{1}{Q_m K_L} \quad (5)$$

$$\ln q_e = \ln K_F + \frac{1}{n} \ln C_e \quad (6)$$

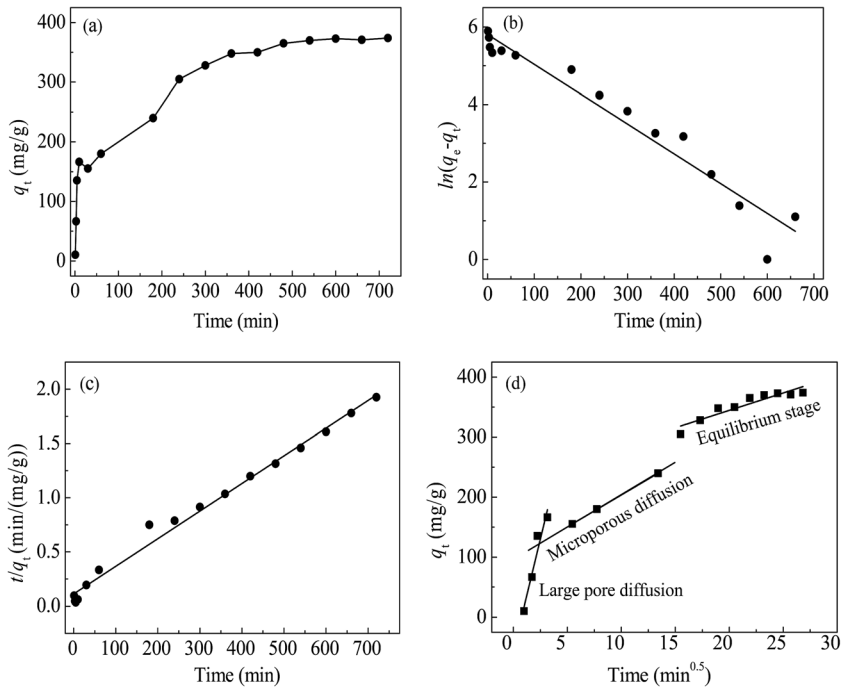

Fig. 10 Adsorption curves of Hg(II) by q_t *vs.* t (a), kinetic fitting of pseudo-first-order (b), pseudo-second-order (c) and intra-particle diffusion (d).

Table 2 Parameters of adsorption kinetics for Hg(II) onto $CoFe_2O_4$@SiO_2–SH

Pseudo-first-order				Pseudo-second-order		
$q_{e,exp}$	$q_{e,cal}$	k_1	R^2	$q_{e,cal}$	k_2	R^2
374.4	332.8	0.0077	0.941	392.2	5.81×10^{-5}	0.989
Intra-particle diffusion						
k_{d1}	C_1	R_1^2	k_{d2}	C_2	R_2^2	k_{d3}	C_3	R_3^2
74.69	−57.21	0.910	10.66	97.06	0.999	5.80	228.39	0.859

where Q_m (mg g^{-1}) is the maximum capacity. K_L (L mg^{-1}), K_F (mg^{1-n} L^n g^{-1}) and n (unitless) are all constants related to adsorption. The separation factor (R_L) can be written as follows:

$$R_L = \frac{1}{1 + K_L C_0} \quad (7)$$

Fig. 11(a) and (b) show the isotherm fitting of Hg(II) on the surface of $CoFe_2O_4$@SiO_2–SH. Table 3 exhibits the isotherm parameters under three temperatures. R^2 (0.995) from Freundlich model was higher than that from Langmuir model (0.989),

Table 3 Isotherm parameters of $CoFe_2O_4$@SiO_2–SH

	Langmuir model				Freundlich model		
T (K)	Q_m	K_L	R^2	R_L	$1/n$	K_F	R^2
298	641.0	0.071	0.989	0.123	0.216	199.5	0.995
308	628.9	0.066	0.991	0.132	0.232	180.8	0.997
318	591.7	0.061	0.987	0.142	0.226	171.1	0.994

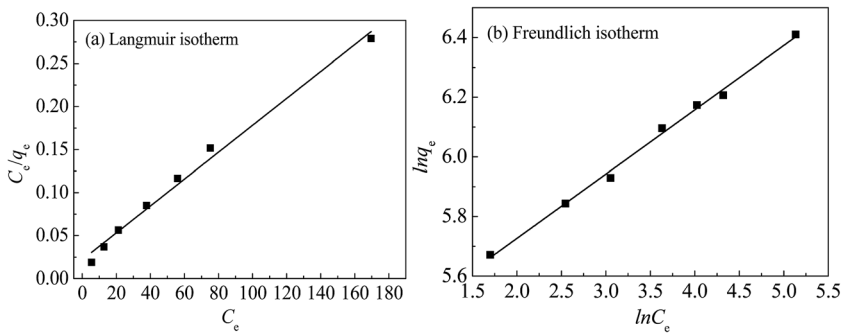

Fig. 11 The Langmuir (a) and Freundlich (b) isotherm curves with $CoFe_2O_4$@SiO_2–SH (T = 298 K, pH = 8, dosage of 0.05 g L^{-1} and t = 12 h).

Table 4 Comparison removal capacity for Hg(II) with various functionalized materials

Materials	pH	Fitting models	Q_m	Ref.
Tannic acid modified Fe_3O_4 core–shell nanoparticles	5	Langmuir isotherm	96	37
Starch/SnO_2	6	Freundlich isotherm	192	38
Polypyrrole/SBA-15	8	Langmuir isotherm	200	39
Amino-functionalized $CoFe_2O_4$–chitosan–graphene	7	Langmuir isotherm	361	40
$CoFe_2O_4$–rGO	4.6	Langmuir isotherm	157.9	41
Magnetic Fe_3O_4 GO	6	Langmuir isotherm	71.3	42
Polystyrene coated $CoFe_2O_4$ modified with 2-(3-(2-aminoethylthio)propylthio) ethanamine	7–8	Langmuir isotherm	84	43
Fe_3O_4@SiO_2–SH	6	Langmuir isotherm	132	44
Mercaptoamine-functionalised silica-coated MNPs	5–6	Freundlich isotherm	355	45
Three types of activated carbons	4	Langmuir isotherm	40–60	46
$CoFe_2O_4$@SiO_2–SH	8	Freundlich isotherm	641.0	This work

indicating a better fitting with Freundlich model compared with Langmuir model. The n from Freundlich constants was greater than 1, indicating a favourable adsorption.[34] Three R^2 from Langmuir model were all greater than 0.980, indicating a good fitting degree. So Langmuir model can be employed to simulate the removal process for Hg(II).

Langmuir also suggested a monolayer adsorption process and the Q_m from $CoFe_2O_4$@SiO_2–SH was 641.0 mg g^{-1}. This value was much larger than the maximum adsorption capacity of many similar materials (Table 4).[35,36] The separation factor R_L can determine if adsorbents have an ability to effectively remove contaminants. The data in Table 3 showed that R_L value changed from 0 to 1, indicating a spontaneous adsorption.

3.5 Adsorption thermodynamics

Three thermodynamic parameters, Gibbs free energy (ΔG°, kJ mol^{-1}) (eqn (8)), enthalpy (ΔH°, kJ mol^{-1}) (eqn (9)) and entropy (ΔS°, kJ mol^{-1} K) (eqn (9)) of adsorption are listed as follows:

$$\Delta G^0 = -RT \ln K_d \quad (8)$$

$$\ln K_d = \frac{\Delta S^0}{R} - \frac{\Delta H^0}{RT} \quad (9)$$

where R is universal gas constant (8.314 J mol^{-1} K), and K_d (q_e/C_e) is a coefficient. The resulted thermodynamic data for Hg(II) removal onto $CoFe_2O_4$@SiO_2–SH was listed in Table 5. For $\Delta H^0 < 0$, the process was exothermic. The value of ΔG^0 was less than 0, indicating that the removal process for Hg(II) was spontaneous.

Table 5 Thermodynamic parameters for Hg(II) removal with $CoFe_2O_4$@SiO_2–SH

			ΔG^0		
C_0	ΔH^0	ΔS^0	298 K	308 K	318 K
40	−0.0116	40.52	−23.68	−24.05	−24.49

3.6 Effect of coexisting ions

In the real application of materials, the anions and cations in the natural water may have an effect on adsorption capacity. Hence, six common types of ions, including three cations (Na^+, K^+ and Ca^{2+}) and three anions (Cl^{-1}, NO_3^- and SO_4^{2-}) were used to assess the removal of Hg(II) with $CoFe_2O_4$@SiO_2–SH.

From Fig. 12, the adsorption properties of materials are affected by the individual ions and decreased as the ionic strength increases. This may be owing to the fact that the cations in the water compete with the active adsorption sites, resulting in a descending adsorption.[47]

Among these ions, Ca^{2+} has the greatest effect on the capacity of materials, probably because Ca^{2+} is a divalent cation with two positive charges, which will occupy two active sites.[48] Therefore, the effect of Ca^{2+} on the performance of the material was larger than that of other monovalent cations including K^+ and Na^+. For anions, Cl^- has the greatest effect on the adsorption. Cl^- can complex with mercury to form $HgCl_2$, $HgCl_3^-$ and $HgCl_4^{2-}$.[43] However, higher concentration of Cl^- can compete for the surface of the active sites with mercury, resulting in a decreased adsorption.[49]

3.7 Application evaluation

In order to further reveal the performance of the material of $CoFe_2O_4$@SiO_2–SH in a real engineering, an application

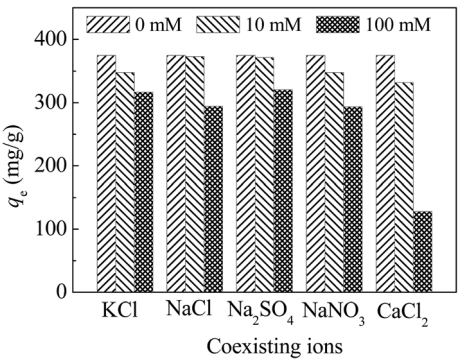

Fig. 12 Effect of coexisting ions and ion strength with $CoFe_2O_4$@SiO_2–SH as adsorbents. Conditions: pH = 8, C_0 = 40 mg L^{-1}, T = 298 K, dosage of 0.05 g L^{-1} and t = 12 h.

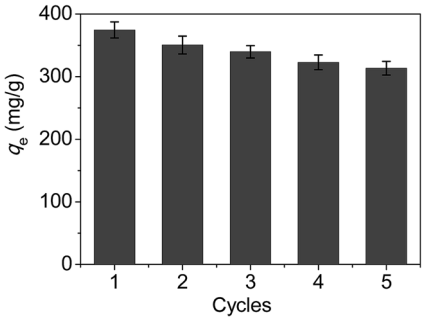

Fig. 13 Adsorption and regeneration cycles of $CoFe_2O_4$@SiO_2–SH.

evaluation was carried out. Firstly, desorption and regeneration experiments were made to investigate the reusable performance of the material, and the results were shown in Fig. 13. From the data in Fig. 13, it can be seen that the adsorption capacities declined slowly with the increasing cycles, and the decrease of adsorption capabilities of $CoFe_2O_4$@SiO_2–SH was about 16.2% after five cycles.

Besides, as we know, electroplating wastewater is a common and typical wastewater and contains many kinds of harmful heavy metals, such as mercury, chromium, nickel, lead, and so on. To investigate the adsorption activity of the material, a real electroplating wastewater sample was employed to be treated by the material of $CoFe_2O_4$@SiO_2–SH.

The concentrations of Hg(II), Cr(VI), Ni(II) and Pb(II) in the wastewater sample are 0.04–0.8 mg L^{-1}, 0.6–1.3 mg L^{-1}, 0.5–1.1 mg L^{-1} and 0.15–0.3 mg L^{-1}, respectively. The COD_{cr} value of wastewater is about 43.5–55.1 mg L^{-1}. The experiments were carried out at the conditions of dosage of 0.15 g L^{-1} and pH of 8 ± 0.2.

The test shows that the removal efficiency of Hg(II) achieved over 99% after adsorption and the effluent basically met the Chinese National Standard "Emission Standard of Pollutants for Electroplating" (GB 21900-2008). The above data indicated that the as-prepared material of $CoFe_2O_4$@SiO_2–SH could be employed as a promising and efficient adsorbent in the real water treatment engineering.

3.8 Mechanism speculation

By comparing the XPS spectra of a wide range and individual important elements of $CoFe_2O_4$@SiO_2–SH before and after adsorption for mercury, it can further investigate the removal mechanism of materials.

Fig. 14(a) exhibits the wide scans of $CoFe_2O_4$@SiO_2–SH (before adsorption) and $CoFe_2O_4$@SiO_2–SH–Hg (after adsorption). Before adsorption, the wide scan clearly shows the peaks of O 1s, C 1s, Si 2p and S 2p. After the material adsorbed Hg(II), the peak of S 2p became weak and the new peaks of Hg 4d and Hg 4p were clearly observed. The presence of Hg 4p and Hg 4f demonstrated the successful adsorption of $CoFe_2O_4$@SiO_2–SH for Hg(II) ions.

Fig. 14(b), through comparing the XPS spectra of S elements before and after adsorption for Hg(II), it can be known that the peak of S 2p after adsorption was weaker than that before adsorption, and was slightly shifted. Also, a peak of S 2p appeared at 162.91 eV before adsorption may belong to –SH.

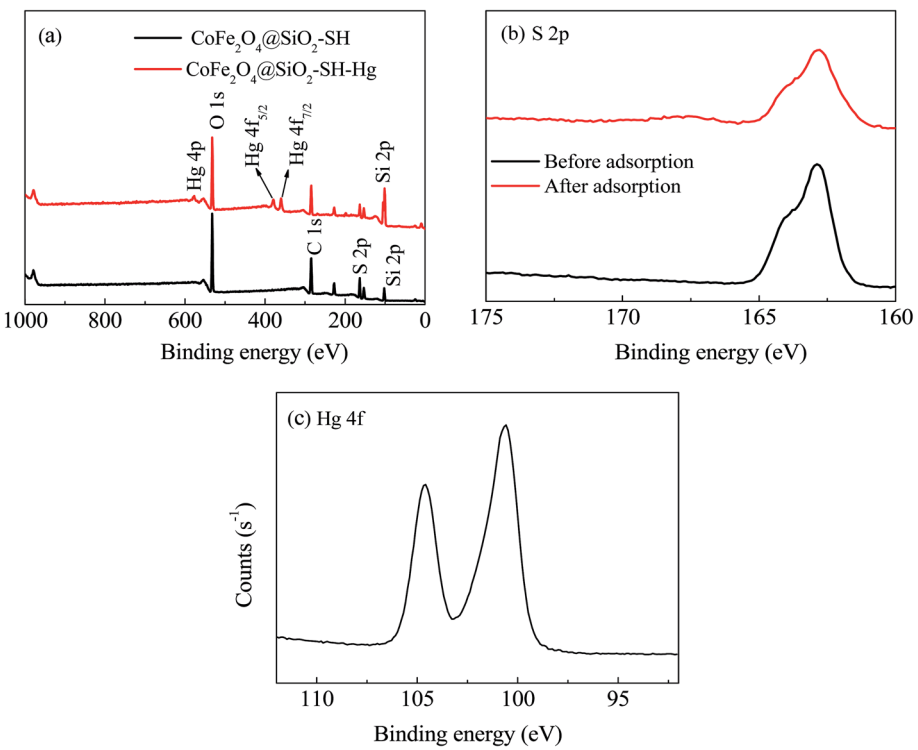

Fig. 14 XPS spectra of wide scan (a), high resolution scan of S 2p (b) before and after adsorption, and Hg 4f (c).

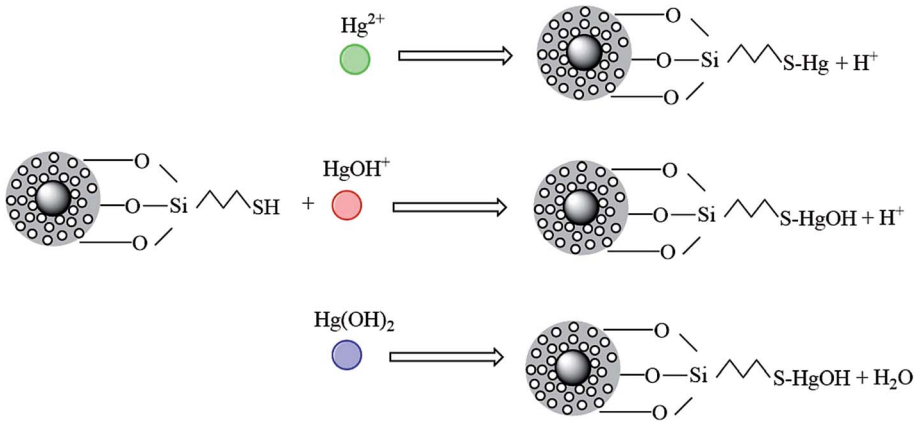

Fig. 15 Diagram of adsorption mechanism.

The peak of S 2p was slightly moved to 162.82 eV after adsorption. It may be that S atoms in mercapto group donated parts of electrons to Hg during the process of adsorption.

From Fig. 14(c), the high resolution XPS spectra of Hg, there is a double-peaks, which may be the Hg $4f_{7/2}$ (100.8 eV) and Hg $4f_{5/2}$ (104.8 eV), which further demonstrates the successful adsorption of mercury onto the material.

As we know, mercury in aqueous solution exists mainly in three forms: Hg^{2+}, $Hg(OH)^{+}$ and $Hg(OH)_2$. In acidic solution (pH < 3), the three forms are all present. Hg^{2+} was the main form of existence, and its amount will decrease with the pH increasing, until disappearance. The amount of the other two forms of $Hg(OH)^{+}$ and $Hg(OH)_2$ will increase as pH increases.

In addition, the number of $Hg(OH)^{+}$ will reach the maximum at pH = 4, and $Hg(OH)_2$ will become the main form at pH > 6. To better understand the removal mechanism, the probable reaction processes between Hg(II) and the mercapto-modified materials are plotted in Fig. 14.

Fig. 15 shows that Hg^{2+} can form –SH–Hg^{+} with the mercapto group under electrostatic attraction, but the existence of large amount of –SH–Hg^{+} might be also slightly prevent the further progress of the reaction. $Hg(OH)^{+}$ and $Hg(OH)_2$ in water can form complexes directly with mercapto groups with/without electrostatic attraction. In the solutions with various pH, the above three forms of mercury exist in different amounts and are adsorbed by the mercapto group by different ways.

In the aforementioned study of pH on adsorption, the gaps between adsorption performances of $CoFe_2O_4$@SiO_2–SH were not large at pH of 2–10. Coupled with results of the effect of mercapto content on the adsorption capacities, it can be concluded that the adsorption capacity of $CoFe_2O_4$@SiO_2 was greatly improved after the introduction of mercapto. $CoFe_2O_4$@SiO_2–SH had an excellent adsorption for mercury, mainly due to the affinity between –SH and mercury, apart from the electrostatic interactions between the material and mercury. Based on the Hard Soft Acid–Base theory, mercapto (soft base) and Hg (soft acid) can have a strong affinity, which is very conducive to the progress of the adsorption reaction.

4. Conclusions

In this study, a thiol-functionalized and silica-coated magnetic nanoparticle ($CoFe_2O_4$@SiO_2–SH) was successfully synthesized *via* a simple and cost effective method, and employed to remove Hg(II) in water.

The adsorption process showed a good performance at pH of 2–10, which implied a probable practical application. And $CoFe_2O_4$@SiO_2–SH had great high adsorption capacities for Hg(II) even with pretty low dosage of 0.05 g L^{-1}.

Kinetic fitting exhibited a good correlation to pseudo-second-order model and adsorption process was controlled by a chemical reaction with three diffusion stages. The isotherm data were in accord with Freundlich model with maximum capacities of 641.0 mg g^{-1} at 298 K and pH of 8, substantially higher than many similar materials. Thermodynamic data displayed an exothermic and spontaneous adsorption process.

Hg^{2+} can form –SH–Hg^{+} with the mercapto group or complexes with/without electrostatic attraction. Furthermore, after adsorption, $CoFe_2O_4$@SiO_2–SH MNPs can be collected from water at a low magnetic field gradient, which helps to prevent secondary pollution and reduce the costs of water treatment. In general, $CoFe_2O_4$@SiO_2–SH MNPs is an economy and efficient material with great potential to remove mercury from water.

Conflicts of interest

There are no conflicts to declare.

Acknowledgements

This work was supported by the National Natural Science Foundation of China (51578354, 51678381), Natural Science Foundation of Jiangsu Province (BK20141179), Six Talent Peaks Program (2016-JNHB-067), Suzhou Science and Technology Bureau (SS201667), Qing Lan Project and Research Innovation Project for College Graduates of Jiangsu Province (SJZZ16_0248, KYCX17_2067).

References

1 T. W. Clarkson, *Crit. Rev. Clin. Lab. Sci.*, 1997, **34**, 369.
2 N. Langford and R. Ferner, *J. Hum. Hypertens.*, 1999, **13**, 651.
3 G. B. Jiang, J. B. Shi and X. B. Feng, *Environ. Sci. Technol.*, 2006, **40**, 3672.
4 M. J. González-Muñoz, M. A. Rodríguez, S. Luque and J. R. Álvarez, *Desalination*, 2006, **200**, 742.
5 W. Plazinski and W. Rudzinski, *Environ. Sci. Technol.*, 2009, **43**, 7465.
6 C. Visvanathan, R. B. Aim and K. Parameshwaranc, *Crit. Rev. Environ. Sci. Technol.*, 2000, **30**, 1.
7 C. H. Mo, Q. Y. Cai and Q. T. Wu, *Chin. J. Appl. Environ. Biol.*, 2001, **7**, 511.
8 H. V. Tran, L. D. Tran and T. N. Nguyen, *Mater. Sci. Eng., C*, 2010, **30**, 304.
9 S. Hokkanen, A. Bhatnagar and M. Sillanpää, *Water Res.*, 2016, **91**, 156.
10 S. Sun, H. Zeng, D. B. Robinson, S. Raoux, P. M. Rice, S. X. Wang and G. Li, *J. Am. Chem. Soc.*, 2004, **126**, 273.
11 Y. X. Ma, D. Xing, C. P. Lu, X. Y. Du and P. Q. La, *Polym. Compos.*, 2016, 9.
12 Z. Wang, J. Xu, Y. Hu, H. Zhao, J. Zhou, Y. Liu, Z. Lou and X. Xu, *J. Taiwan Inst. Chem. Eng.*, 2016, **60**, 394.
13 Y. Ma, P. La, W. Lei, C. Lu and X. Du, *Desalin. Water Treat.*, 2016, **57**, 5004.
14 S. X. Zhang, H. Y. Niu, Y. Cai, X. L. Zhao and Y. Shi, *Chem. Eng. J.*, 2010, **158**, 599.
15 C. Ren, X. Ding, H. Fu, C. Meng, W. Li and H. Yang, *RSC Adv.*, 2016, **6**, 72479.
16 R. Roto, Y. Yusran and A. Kuncaka, *Appl. Surf. Sci.*, 2016, **377**, 30.
17 O. Fardmousavi and H. Faghihian, *C. R. Chim.*, 2014, **17**, 1203.
18 J. Zhu, J. Yang and B. Deng, *J. Hazard. Mater.*, 2009, **166**, 866.
19 S. Zhang, H. Niu, Y. Cai, X. Zhao and Y. Shi, *Chem. Eng. J.*, 2010, **158**, 599.
20 B. Viltužnik, A. Košak, Y. L. Zub and A. Lobnik, *J. Sol-Gel Sci. Technol.*, 2013, **68**, 365.
21 O. Hakami, Y. Zhang and C. J. Banks, *Water Res.*, 2012, **46**, 3913.
22 S. Dong, X. Dou, D. Mohan, C. U. Pittman Jr and J. Luo, *Chem. Eng. J.*, 2015, **270**, 205.
23 Y. Zhang, Q. Xu, S. Zhang, J. Liu, J. Zhou, H. Xu, H. Xiao and J. Li, *Sep. Purif. Technol.*, 2013, **116**, 391.
24 G. Li, Z. Zhao, J. Liu and G. Jiang, *J. Hazard. Mater.*, 2011, **192**, 277.
25 H. Parham, B. Zargar and R. Shiralipour, *J. Hazard. Mater.*, 2012, **205–206**, 94.
26 S. Zhang, Y. Zhang, J. Liu, Q. Xu, H. Xiao, X. Wang, H. Xu and J. Zhou, *Chem. Eng. J.*, 2013, **226**, 30.
27 L. C. Lin, M. Thirumavalavan and J. F. Lee, *Clean: Soil, Air, Water*, 2015, **43**, 775.
28 Y. Sun, X. Ding, Z. Zheng, X. Cheng, X. Hu and Y. Peng, *Eur. Polym. J.*, 2007, **43**, 762.
29 Y. S. Ho and G. Mckay, *Water Res.*, 1999, **33**, 578.
30 Y. S. Ho and G. Mckay, *Process Biochem.*, 1999, **34**, 451.
31 M. Yari, M. Rajabi, O. Moradi, A. Yari, M. Asif, S. Agarwal and V. K. Gupta, *J. Mol. Liq.*, 2015, **209**, 50.
32 I. Langmuir, *J. Chem. Phys.*, 1918, **40**, 1361.
33 M. D. Levan and T. Vermeulen, *J. Phys. Chem.*, 1981, **85**, 3247.
34 L. Zhou, L. Ji, P. C. Ma, Y. Shao, H. Zhang, W. Gao and Y. Li, *J. Hazard. Mater.*, 2014, **265**, 104.
35 Y. S. Bo, Y. Eom and G. L. Tai, *Appl. Surf. Sci.*, 2011, **257**, 4754.
36 B. Viltužnik, A. Lobnik and A. Košak, *J. Sol-Gel Sci. Technol.*, 2015, **74**, 199.
37 H. Luo, S. Zhang, X. Li, X. Liu, Q. Xu, J. Liu and Z. Wang, *J. Taiwan Inst. Chem. Eng.*, 2017, **72**, 163.
38 M. Naushad, T. Ahamad, G. Sharma, A. A. H. Al-Muhtaseb, A. B. Albadarin, M. M. Alam, Z. A. Alothman, S. M. Alshehri and A. A. Ghfar, *Chem. Eng. J.*, 2016, **300**, 306.
39 M. Shafiabadi, A. Dashti and H. A. Tayebi, *Synth. Met.*, 2016, **212**, 154.
40 Y. Zhang, T. Yan, L. Yan, X. Guo, L. Cui, Q. Wei and B. Du, *J. Mol. Liq.*, 2014, **198**, 381.
41 Y. Zhang, L. Yan, W. Xu, X. Guo, L. Cui, L. Gao, Q. Wei and B. Du, *J. Mol. Liq.*, 2014, **191**, 177.
42 Y. F. Guo, J. Deng, J. Y. Zhu, X. J. Zhou and R. B. Bai, *RSC Adv.*, 2016, **6**, 82523.
43 K. Jainae, N. Sukpirom, S. Fuangswasdi and F. Unob, *J. Ind. Eng. Chem.*, 2014, **23**, 273.
44 Z. Wang, J. Xu, Y. Hu, H. Zhao, J. Zhou, Y. Liu, Z. Lou and X. Xu, *J. Taiwan Inst. Chem. Eng.*, 2016, **60**, 394.
45 S. Bao, K. Li, P. Ning, J. Peng, X. Jin and L. Tang, *Appl. Surf. Sci.*, 2016, **393**, 457.
46 Y. F. Guo, Z. Wang, X. J. Zhou and R. B. Bai, *Res. Chem. Intermed.*, 2016, **10**, 1.
47 L. Cui, Y. Wang, L. Gao, L. Hu, Q. Wei and B. Du, *J. Colloid Interface Sci.*, 2015, **456**, 42.
48 L. Tran, P. Wu, Y. Zhu, Y. Lin and N. Zhu, *J. Colloid Interface Sci.*, 2015, **445**, 348.
49 M. M. Benjamin and J. O. Leckie, *Environ. Sci. Technol.*, 1982, **16**, 162.